

See discussions, stats, and author profiles for this publication at: <https://www.researchgate.net/publication/280940633>

Chain-Stiffness-Induced Entropy Effects Mediate Interfacial Assembly of Janus Nanoparticles in Block Copolymers: From Interfacial Nanostructures to Optical Responses

ARTICLE *in* MACROMOLECULES · JULY 2015

Impact Factor: 5.8 · DOI: 10.1021/acs.macromol.5b01290

READS

96

4 AUTHORS, INCLUDING:



Zihan Huang

Tsinghua University

6 PUBLICATIONS 7 CITATIONS

SEE PROFILE

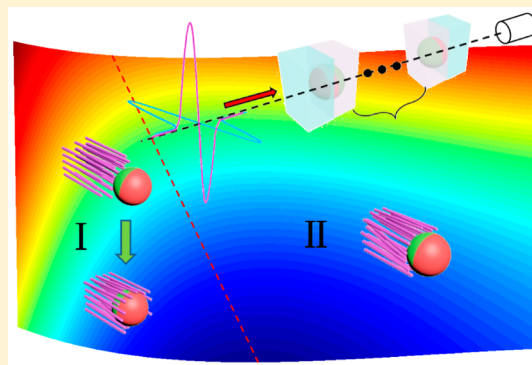
Chain-Stiffness-Induced Entropy Effects Mediate Interfacial Assembly of Janus Nanoparticles in Block Copolymers: From Interfacial Nanostructures to Optical Responses

Bojun Dong, Zihan Huang, Honglin Chen, and Li-Tang Yan*

Key Laboratory of Advanced Materials (MOE), Department of Chemical Engineering, Tsinghua University, Beijing 100084, P. R. China

Supporting Information

ABSTRACT: Understanding entropic contributions to ordering transitions is essential for the design of self-assembling systems with tunable hierarchical structures. Herein, we report entropy-mediated precise interfacial organization of Janus nanoparticles in the flexible–semiflexible block copolymers and the resulted optical properties of this heterogeneous material by combining coarse-grained molecular dynamics and a finite difference time domain technique. We find that the stiffness of the semiflexible block can regulate the off-center distribution of symmetric Janus nanoparticles with respect to phase interfaces, featured by a roughly 35% deviation from the interface to the utmost extent. Our simulations reveal how entropic and enthalpic effects in this multiphase media contribute to the self-assembled morphologies and, in particular, can lead to novel chain stiffness-induced entropy effects that can be harnessed to tailor the interfacial organization of Janus nanoparticles in the scaffold of block copolymers. Furthermore, the combination of techniques allows us to determine how changes of the interfacial nanostructures affect the optical properties of the nanocomposite. The findings enable the applications of polymer chain stiffness in precise control over the interfacial assembly of nanoparticles in heterogeneous materials and provide guidelines for facilitating the design of photonic crystals.



INTRODUCTION

Hierarchical control over the spatial organization of nano building blocks, such as nanoparticles, has been a major challenge in the “bottom-up” generation of technologically important materials.^{1–9} Various routes to direct nanoparticles assemblies have been explored, including the use of DNA^{10–13} and functional polymers.^{1,14–19} Nanoparticles arrays with tunable symmetry and dimensionality can form through programmable self-assembly of tailor-made building blocks with DNA linkers.^{10–13} However, large-scale fabrication of these building blocks poses a significant hurdle for many practical applications.²⁰ Self-assembling of block copolymers, on the other hand, offers alluring opportunities to generate exquisitely tailored materials with effective control over nanoscale-domain geometry, packing symmetry, and chemical positions, making them ideal scaffolds for directing the assembly of nanoparticles.^{16,17,21–28} Of particular interest is the control of the assembly of nanoparticles at the interface between different phase domains.^{29–33} Janus nanoparticles consisting of two compartments of different chemistry or polarity are ideal building blocks to generate tunable and stable interfacial nanostructures because the Janus character of these nanoparticles provides them with tailorable surface and a higher interfacial activity compared with homogeneous nanoparticles.³⁴

However, precise control of such interfacial nanostructures still remains a challenge because the interfacial organization of Janus nanoparticles in block copolymers is governed by an intricate balance of entropic and enthalpic interactions.^{1,16,18,27,28} Central to this issue is exploring entropy-driven structural organization because entropy keeps springing nonintuitive findings in the manipulation of the self-assembly of nanoparticles and the structural formation of soft matter systems.^{18,35–40} In fact, understanding entropic contributions to ordering transitions is essential for the design of self-assembling systems with tunable hierarchical structures.^{35,36} Various unexpected hierarchical structures can form by self-assembly of tailor-made building blocks, and these can be designed so that such structures increase the entropy of the system.^{37–40} Indeed, over the past few decades examples have been highlighted in which entropic interactions are exploited to direct the self-assembled morphologies of nanoparticles in polymers.^{1,37,40} Despite these successes, establishing principles of entropy-driven *interfacial* assembly of nanoparticles and thereby controlling the macroscopic performance of resulted polymer nanocomposites remain a challenge.

Received: June 13, 2015

Published: July 28, 2015

Here we report novel entropic effects that arise from the chain stiffness of the semiflexible block in the flexible–semiflexible block copolymers and can be harnessed to tailor the precise interfacial organization of Janus nanoparticles in such polymer scaffolds. Our simulations demonstrate that the stiffness of the semiflexible block can regulate the off-center distribution of symmetric Janus nanoparticles with respect to the phase interface, featured by a roughly 35% deviation from the interface to the utmost extent. The results reveal how entropic and enthalpic effects in this multiphase media contribute to the self-assembled morphologies and, in particular, can lead to entropically driven spatial transition of interfacial nanostructures. Furthermore, by combining self-assembled morphological studies conducted by coarse-grained molecular dynamics (CGMD) and a finite difference time domain (FDTD) technique, we can see how changes of the interfacial nanostructures affect the optical properties, such as the band gaps and the principal frequency, of the nanocomposites. To the best of our knowledge, this is the first simulation study to capture the chain stiffness-dependent structural transition in the interfacial assembly of nanoparticles and offers guidelines for facilitating the design of photonic band gap materials.

METHODOLOGY

Determining the Self-Assembled Morphologies. CGMD simulations based on the dissipative particle dynamics (DPD) method are performed to investigate the self-assembled morphologies.⁴¹ DPD is a powerful mesoscopic tool that can be used for modeling physical phenomena occurring at larger time and spatial scales than typical MD as it utilizes a momentum-conserving thermostat and soft repulsive interactions between the beads representing clusters of molecules. In our DPD simulations, we consider the mixtures of AB diblock copolymers filled with spherical Janus nanoparticles. Beyond the traditional nanoparticle organization in flexible copolymers, flexible–semiflexible copolymers are considered in the present work where block A is flexible but block B semiflexible with tunable chain stiffness. A flexible–semiflexible A₆B₆ diblock copolymer, which can self-assemble into a lamellar nanostructure, is chosen in the simulations, where the neighboring beads are connected by bonds. These bonds are represented by a harmonic spring potential $U_{\text{bond}} = K_b((r - b)/r_c)^2$, where $K_b = 64k_B T$ and $b = 0.5r_c$ are the bond constant and the equilibrium bond length respectively (r_c : the length unit of DPD). Additionally, we include a three-body stiffness potential along the semiflexible B block of the form $U_{\text{angle}} = (K_a/2)(\cos(\theta) - \cos(\theta_0))^2$.⁴² Various values of K_a are used to mimic the change of the chain stiffness of block B. The correlation between K_a and the persistence length of polymer chain, l_p , is calculated and shown in Figure S1.⁴³ Each Janus nanoparticle consists of two sites with equal surface areas.²⁸ The radius of Janus nanoparticles is fixed at $R_n = 1.11r_c$ and a low volume fraction of nanoparticles, i.e., $V_p = 0.02$, is chosen so that the effect of the particle–particle interaction is trivial.

The present simulations are carried out using four different interaction forces between beads, i.e., the conservative interaction force F^C , dissipative force F^D , random force F^R , and spring force F^S . The interaction forces are treated as pairwise additive. The detailed forms of F^C , F^D , and F^R , which can be found elsewhere, are of short-range with a fixed cutoff distance, r_c .⁴¹ In DPD, the interaction strength between beads i and j is determined by the maximum repulsion parameter in the

formula of the conserved force, α_{ij} , which has a linear relationship with Flory–Huggins χ parameter: $\chi_{ij} \approx (\alpha_{ij} - \alpha_{ii})/3.27$. $\alpha_{ii} = 25 k_B T$ is the interaction between like species (i.e., $\chi_{ii} = 0.0$). In the present simulations, $\chi_{AB} = 6.0$, $\chi_{PQ} = 7.6$, $\chi_{AQ} = 1.1$, and $\chi_{AP} = \chi_{BQ} = 0.0$ are set for various interactions where A, B represent the beads of the two blocks of block copolymers and P, Q indicate the beads of two compartments of Janus nanoparticles. Clearly, the A and B blocks have strong affinities to the P and Q sites of Janus nanoparticles, respectively. The repulsion between B and P, $\chi_{BP} = 0.15$, is set except where noted otherwise. All simulations are carried out in the canonical ensembles using a modified velocity-Verlet integration algorithm with a time step $\Delta t = 0.01\tau$ where τ is the time unit of DPD. The simulation box is $(20r_c)^3$ in size and with periodic boundary condition in all directions, which is large enough to avoid the finite size effect. Each structure is determined over three independent runs, and each run is equilibrated with more than 5 million time steps.

Determining the Optical Properties. A FDTD technique enables the optical investigation of the Janus nanoparticle–block copolymer nanocomposite to be undertaken. FDTD is a flexible, numerical means of analyzing interactions between waves and complex materials containing electric or metallic objects.⁴⁴ This technique is particularly useful for examining the behavior of heterogeneous materials since one can readily compute the propagation of light in materials that containing particles of arbitrary shape or interparticle distance. In the FDTD technique, the coupled Maxwell's equations in the differential form are solved for various points of the scatters as well as its surroundings in a time-stepped manner until converged solutions are obtained. The differential form of Maxwell's time-dependent curl equations can be written as follows:⁴⁵

$$\nabla \times \bar{E} = -\mu \frac{\partial \bar{H}}{\partial t} \quad (1)$$

$$\nabla \times \bar{H} = \epsilon \frac{\partial \bar{E}}{\partial t} + \sigma \bar{E} \quad (2)$$

where \bar{E} and \bar{H} are respectively the electric and the magnetic fields that are positioned at half-step interval around a unit cell. The parameters σ , μ , and ϵ are the conductivity, permeability, and permittivity.

In the rectangular coordinate system (x , y , z), the following system of scalar equations is equivalent to the x components of the Maxwell's equations

$$\frac{\partial E_x}{\partial t} = \frac{1}{\epsilon} \left(\frac{\partial H_z}{\partial y} - \frac{\partial H_y}{\partial z} - \sigma E_x \right) \quad (3)$$

$$\frac{\partial H_x}{\partial t} = \frac{1}{\mu} \left(\frac{\partial E_y}{\partial z} - \frac{\partial E_z}{\partial y} \right) \quad (4)$$

Similar expressions can be written for the y and z components. The detailed discretization forms of these equations on the “Yee cells” can be found in Supporting Information. For the boundary conditions, the perfectly match layer (PML) is used to generate free space boundary conditions of the simulation domain.⁴⁶

To carry out our studies of the optical properties, the self-assembled morphologies are first obtained through the DPD simulations. The output of this CGMD model then serves as the input to estimate the local dielectric constants at the center of mesh cells in the FDTD simulation. The total dielectric

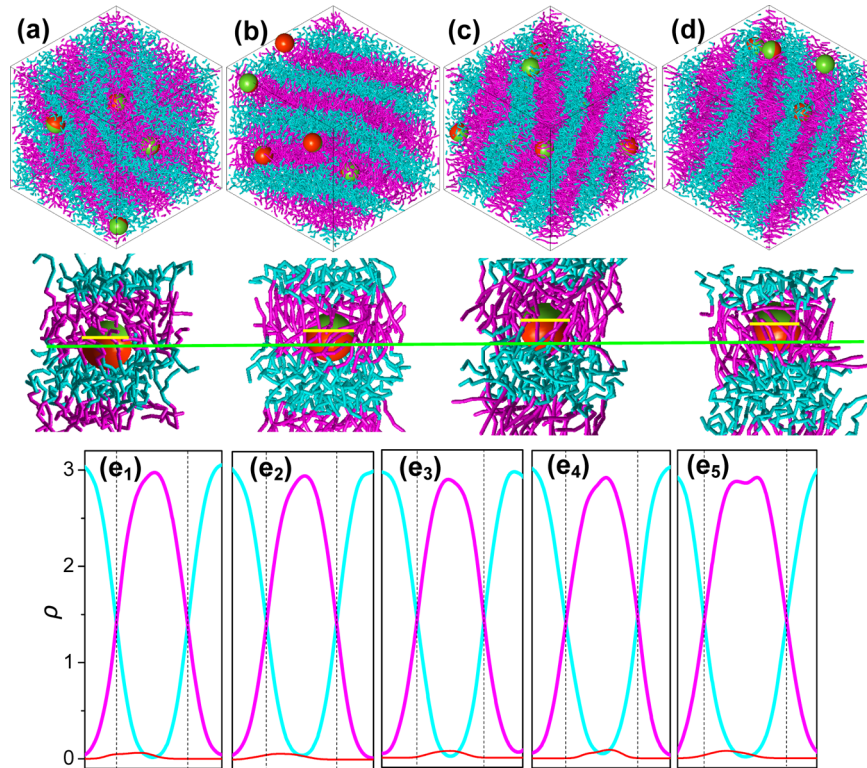


Figure 1. (A–D) Representations of the self-assembly of Janus nanoparticles in AB diblock copolymers with flexible A block but stiff B block of various stiffness: (a) $K_a = 0 \text{ } k_B T$, (b) $K_a = 40 \text{ } k_B T$, (c) $K_a = 100 \text{ } k_B T$, and (d) $K_a = 300 \text{ } k_B T$. At each K_a , the top snapshot shows the self-assembled morphologies where the cyan and pink chains denote blocks A and B, and sites P and Q of every Janus nanoparticle are colored red and yellow, respectively; the bottom snapshot highlights the detailed position of a Janus nanoparticle at the interface and the conformation of the polymer chains around it. The green and yellow lines mark the phase interface and the equator of the nanoparticle. (e₁–e₅) The density profiles of blocks A (cyan) and B (pink), and the Janus nanoparticle (red) for various stiffness of block B: (e₁) $K_a = 5 \text{ } k_B T$, (e₂) $K_a = 40 \text{ } k_B T$, (e₃) $K_a = 60 \text{ } k_B T$, (e₄) $K_a = 100 \text{ } k_B T$, and (e₅) $K_a = 400 \text{ } k_B T$.

constant at each point is obtained by linearly weighting the contributions of the different components based on the respective volume fractions, i.e., $\epsilon(\mathbf{r}) = \Phi_A(\mathbf{r})\epsilon_A + \Phi_B(\mathbf{r})\epsilon_B + \Phi_P(\mathbf{r})\epsilon_P$, where ϵ_i denotes the permittivity of component i . In the current simulations, the dielectric constants for blocks A and B are set as 2.28 and 2.53, falling in the range that is typical for polymeric materials.⁴⁷ The dielectric constant of the nanoparticles is set as 10.2, corresponding to the value for cadmium selenide.⁴⁸ In order to establish a correlation between simulation parameters and experimental values, and thus set up a physical length scale in our system, we equate the thickness of a lamellar domain obtained from the CGMD for the pure symmetric diblock to 50 nm. Also, to capture the detailed dependence of the optical properties on the self-assembled morphologies, we enlarge the number of the lamellar domains to 50 in the x direction. These layers are then sandwiched between two homogeneous regions of a dielectric constant equal to that of the pure A phase component, ensuring that the reflection of light when radiated on the multilayered structure depends on the self-assembled morphologies.

RESULTS AND DISCUSSION

Interfacial Nanostructures. Figure 1a–d displays some representative snapshots showing the self-assembled morphologies of symmetry Janus nanoparticles in the A_6B_6 diblock copolymers where the stiffness of the B block is gradually enhanced by increasing K_a from 0 to $300 \text{ } k_B T$. Within the range of K_a , the flexible–semiflexible block copolymers present

lamellar structure with Janus nanoparticles anchored at the phase interfaces. The chain model allows us to identify the detailed conformation of the block segments in their domains: the semiflexible B block segments tend to orient along a predominant direction with the increase of K_a , in contrast to the random-coil state of the flexible A block segments (see Figure S3 for more detailed structures). With respect to capturing the stiffness-dependent behavior of the detailed spatial distribution of Janus nanoparticles at interfaces, a single Janus nanoparticle with polymer chains around it has been extracted out from each system, as demonstrated by the bottom images in Figure 1a–d. What is striking is that the equator of the symmetry Janus nanoparticles deviates from the phase interface to the domain of semiflexible block B. Moreover, the off-center distribution becomes more evident when K_a is increased from 0 to $100 \text{ } k_B T$ while the Janus particle turns to return to the interface for a larger stiffness at $300 \text{ } k_B T$ (Figure 1d). The change of the interfacial distribution of Janus nanoparticles can be further confirmed through examining the density profiles of different components (Figure 1e₁–e₅). Indeed, the peak of the profile of Janus nanoparticles presents the same changing rule with that demonstrated by Figure 1a–d upon increasing the chain stiffness of B block segments.

To determine the detailed stiffness-dependent behavior of the interfacial nanostructures, we quantify the precise position of Janus nanoparticles with respect to interfaces by the fraction of Janus nanoparticle surface wrapped by the beads of A segment, f_w . $f_w = 0.5$ indicates that the center of a Janus

nano particle coincides exactly with the interface while a smaller f_w denotes that its center deviates from the interface and is positioned at the B phase, and vice versa. In the present work, each structure is determined over three independent runs, and its f_w is obtained through averaging the values from these different runs. Taking K_a values from 0 to 1000 $k_B T$, we give the plot of f_w as a function of K_a (for detailed self-assembled morphologies of each point see Figure S4). The insetting diagrams of Figure 2 scheme the position of a Janus nanoparticle relative

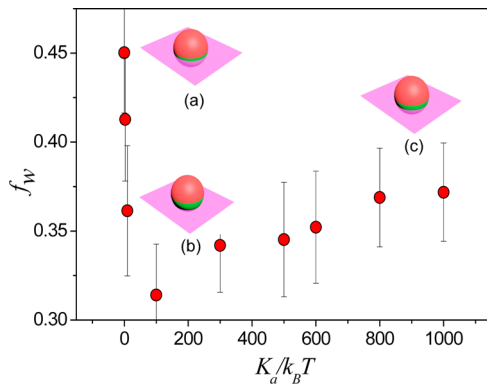


Figure 2. Dependence of the spatial distribution of Janus nanoparticles on the stiffness of block B. f_w is the fraction of the Janus nanoparticle surface wrapped by block A. The insetting schematic diagrams illustrate the position of Janus nanoparticle with respect to the phase interface at $K_a = 0 k_B T$ (a), $100 k_B T$ (b), and $800 k_B T$ (c).

to the interface at different K_a . Interestingly, one can find a crossover occurring at about $150 k_B T$ in the $f_w - K_a$ plot. Before the crossover, f_w is dramatically reduced with the increase of K_a , revealing that a mild increase in the chain stiffness of the B block segment causes the Janus nanoparticles to significantly deviate from the interface and to migrate to the B domains. Subsequent to the crossover, f_w however turns to slightly increase for a larger K_a . In this case, the off-center distribution is alleviated as the Janus nanoparticles tend to return to the interface.

For the purpose of demonstrating the generality of such a stiffness-dependent behavior of the interfacial nanostructures, we systematically compute the wrapping degree f_w as a function of K_a and the interaction parameter between B segments and P site of Janus nanoparticles, χ_{BP} , which allows us to construct the f_w landscape plotted by the colored contour map in the $\chi_{BP} - K_a$ plane (Figure 3). The points where independent runs are performed to generate the contour map have been listed in Figure S5. Figure 3 clarifies a strong dependence of the interfacial distribution of nanoparticles on the chain stiffness of the B block segments. Particularly, two characteristic regions can be identified in the map, as approximately separated by the dashed line. In regime I with low stiffness of B block segments, a mild increase of K_a can dramatically reduce the value of f_w . By contrast, in regime II, further increasing the value of K_a turns to result in larger values of f_w . Indeed, the calculation results reproduce the rule demonstrated in Figures 1 and 2 and consequently highlight the generality of the stiffness-dependent behavior, although a higher value of χ_{BP} points to a crossover at lower chain stiffness. Notably, the color bar clarifies that the lowest wrapping degree f_w even reaches roughly 35%, being a significant deviation of Janus nanoparticles toward the domain of the stiff block segments. Clearly, the interfacial nanostructures can be regulated through changing the stiffness of the

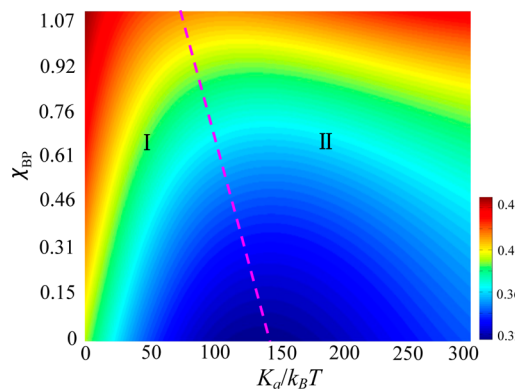


Figure 3. Contour map plots the wrapping degree, f_w , in the plane of χ_{BP} and K_a . The dashed pink line indicates the approximate boundary between two regimes. The color bar indicates the value of f_w . The variance at each calculation point is about 0.03.

block segments. These results thereby suggest an effective approach for precise control over the interfacial assembly^{29–33} of nanoparticles by virtue of tailored molecular architectures, especially the chain stiffness, of polymer scaffolds.

Chain-Stiffness-Induced Entropic Effects. Physically, the assembly of Janus nanoparticles with block copolymers is determined by a combination of enthalpic and entropic contributions. To gain a detailed insight into the entropic contribution of the stiff segments to the position deviation of Janus nanoparticles, we turn to the excess entropy defined as the difference between the thermodynamic entropy and the entropy of the ideal gas under the same temperature and density conditions.⁴⁹ The two-body approximation on the basis of pair correlation function (PCF) has been demonstrated to provide a reasonable estimation of the total excess entropy.⁵⁰ We herein calculate excess entropy per bead, S_{BB} , from the PCF between B-segment beads as follows:

$$S_{BB} = -2\pi \int \{g_{BB}(z) \ln g_{BB}(z) - [g_{BB}(z) - 1]\} z^2 dz \quad (5)$$

Here $g_{BB}(z)$ denotes the PCF between B-segment beads and is listed in Figure S6 as an example.

For the flexible polymer chains, the interaction between nanoparticles and their neighboring polymer chains has been demonstrated to incur a loss of conformational entropy of the coiled chains since they must stretch around the nanoparticles to accommodate these solids [schematic diagram (a) in Figure 4].¹⁶ However, the conformational transition of semiflexible polymer chains becomes very difficult due to the barrier from the chain stiffness; rather, these block segments exhibit long-range orientational order in their phase domain (Figure 1b–d, Figures S3 and S4). The orientational order of rigid molecules with high aspect ratio has been found to be very common, certainly in the systems of liquid crystals.^{51–53} Although the orientational transition lowers the steric repulsion between the stiff blocks, such an ordering transition results in a significant entropic loss of the B segments, as demonstrated by the dramatic decrease of S_{BB} before $K_a \sim 150 k_B T$ in the $S_{BB} - K_a$ plot (Figure 4). This is not difficult to be understood: the ordering transition leads to an approximately uniform orientation of the stiff block segments yet restrains other possible orientational states of every segment [schematic diagram (b) in Figure 4]. To disrupt such orientational ordering and thereby increase the entropy, Janus nanoparticles deviate from phase interfaces and migrate

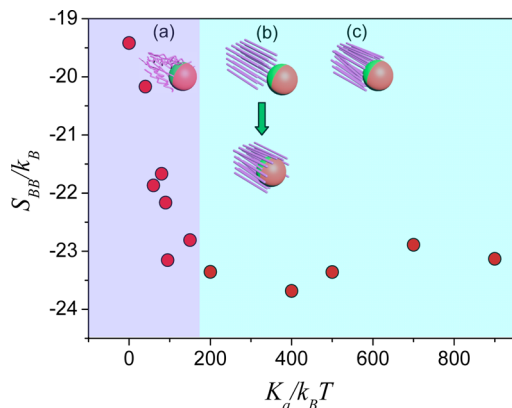


Figure 4. K_a dependence of the excess entropy per bead, S_{BB} , calculated from the pair correlation function between B-block beads. The insetting diagrams (a)–(c) scheme the position of Janus nanoparticles and the organization of the stiff B blocks around it in response to the increase of the chain stiffness.

to the domain of the stiff block segment, as illustrated by schematic diagram (b) and corroborated by the simulation results of Figures 1–3. The off-center distribution from the interface drives a considerable fraction of the P site of Janus particles into the chemically incompatible B phase domain; thus, chain-stiffness-induced entropic effects overwhelm the unfavorable enthalpic interactions.

Figure 4 also shows that further increase of the chain stiffness of B segments turns to induce a slight increase of S_{BB} . This can be rationalized as a consequence of the packing frustration of the semiflexible block segments with very high stiffness, which is manifested by the curved phase interfaces and will be quantified and discussed in more detail in the following section. Such

packing frustration offers more translational entropy for the more persistent B block segments, partly offsetting the entropic loss caused by the extreme orientational ordering of the stiff segments. In this case, the requirement for the entropic contribution due to the off-center shifting of Janus nanoparticles is alleviated [schematic diagram (c) in Figure 4]. Janus nanoparticles thereby cross over to return to the interface with further increasing the stiffness of the B segments from a critical value of K_a , accounting for the corresponding simulation results demonstrated in Figures 1–3.

Interfacial Fluctuation. To elucidate the dependence of packing frustration of semiflexible block segments on the chain stiffness, a quantitative description of the fluctuation of the curved phase interfaces is required. Here we capture the interfacial fluctuation by measuring averaged curvature of the interfaces according to a shape-fitting protocol as follows.⁵⁴ First of all, a lamellar domain of B block segments is extracted out of the bulk, facilitating us to further refine its interfacial beads (Figure 5a,b). The interface is divided into $0.1r_c \times 0.1r_c$ vertical square prisms, and interfacial beads within each square prism are averaged to determine the centers of mass of the prism. The data are then collected to construct a geometric surface as a smooth resolution of the interface shape (Figure 5c). In order to calculate conveniently the curvature at each position of the surface, the geometric surface should be further fitted according to a certain formula. In the present work, the best-fitted surface of the phase interface via least-squares fitting of the geometric surface is described in the form of the quintic polynomial; that is $z(x,y) = \sum_{i+j \leq 5} a_{ij} x^i y^j$, where the coefficients a_{ij} are free parameters determined during the fitting. Figure 5d shows the best-fitted surface of the phase interface, and a close comparison confirms the effective fluctuation correlation between interfacial beads and the best-fitted surface (Figure S7). Once the best-fitted surface is

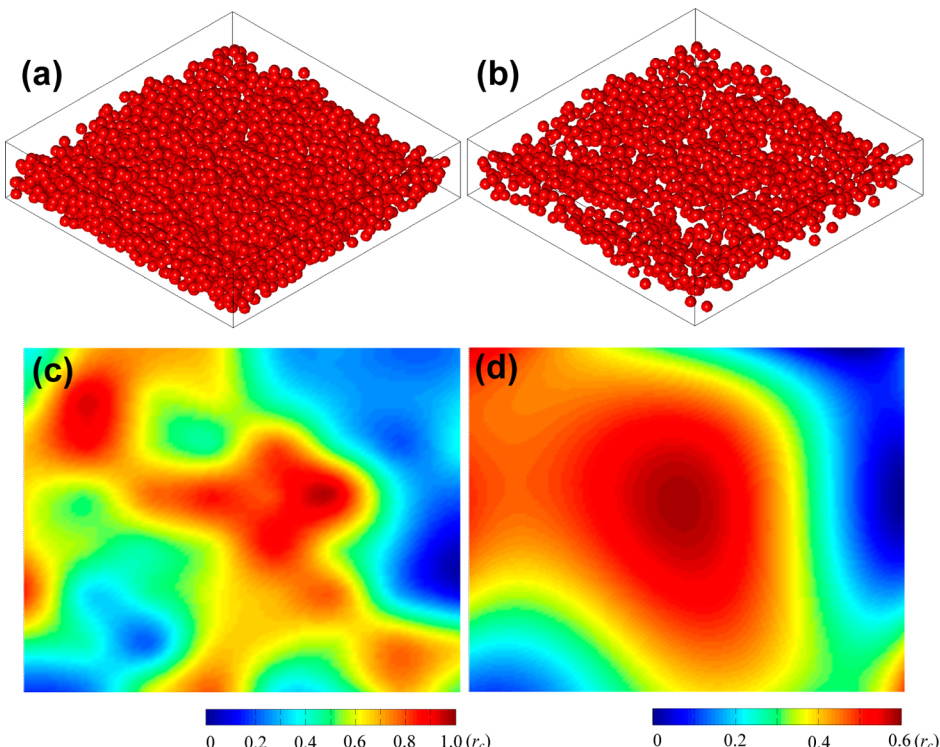


Figure 5. Shape-fitting of the phase interface. (a) Phase B shown by DPD beads at $K_a = 500 k_B T$. (b) Interfacial beads extracted from (a). (c) Geometric surface of the phase interface. (d) Best-fitted surface of the phase interface.

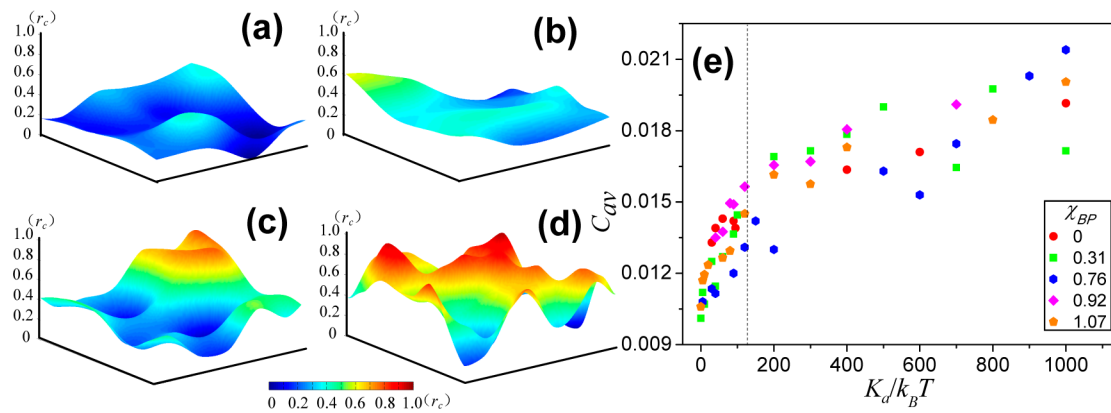


Figure 6. (a–d) Geometric surfaces at different K_a showing the dependence of interfacial fluctuation on the stiffness of block B: (a) $K_a = 10 k_B T$, (b) $K_a = 60 k_B T$, (c) $K_a = 250 k_B T$, and (d) $K_a = 500 k_B T$. (e) Averaged curvature of the interfacial surface, C_{av} , as a function of K_a at various χ_{BP} .

determined, curvature radii at point (x, y) along the x and y directions, r_x and r_y , can be readily evaluated via the following expressions:

$$r_x = \left[1 + \left(\frac{dz}{dx} \right)^2 \right]^{3/2} / \frac{d^2z}{dx^2}, \quad r_y = \left[1 + \left(\frac{dz}{dy} \right)^2 \right]^{3/2} / \frac{d^2z}{dy^2} \quad (6)$$

The curvature at this point can be calculated in terms of eq 6, and the averaged curvature of the whole interface, C_{av} , is further obtained through a surface average of the curvature at each point of the best-fitted surface.

Figure 6a–d shows three-dimensional diagrams of the geometric surfaces demonstrating the interface fluctuation upon increasing the chain stiffness of the B block segments. We also present the C_{av} – K_a plots for various χ_{BP} in Figure 6e. The figures manifest that the averaged curvature of phase interface is relatively slight although it undergoes a dramatic increase when K_a is not larger than about $150 k_B T$. Further increasing K_a however gives rise to evident interfacial fluctuation, indicating that the interface becomes sharp. These results corroborate the fact that packing frustration of more persistent B block segments dominates the behavior of the system as advantage can be taken of the translation entropy of these extremely stiff segments. The interfacial fluctuation leads to free energy gain partly offsetting the loss of the conformational entropy caused by the orientational ordering of the stiff segments. As a consequence, the off-center shifting of Janus nanoparticle is alleviated due to less entropic contribution is required from such an enthalpically unfavorable interfacial deviation. Additionally, the topology of the fluctuating interface may be another important factor accounting for the reduced wrapping degree, if considering that a topology mismatching will always arise when the symmetry Janus nanoparticle is placed at a curved interface.⁵⁵

Kinetic Pathway. To gain an in-depth insight into the formation mechanism of off-center interfacial distribution of Janus nanoparticles in the flexible–semiflexible block copolymers, in Figure 7 we present a typical kinetics pathway where the polymer nanocomposite evolves from an initially random state to the ordered lamellar structure. For the purpose of delineating the detailed kinetics of interfacial organization, a certain Janus nanoparticle with polymer chains around it is extracted out of the system, as demonstrated by the bottom image at each time. One can find that the orientation of Janus nanoparticle undergoes evident fluctuation accompanying with

the structural evolution of the block copolymers. A close examination of the single nanoparticle and its surrounding chains reveals that the orientation of the Janus nanoparticle basically coincides with the concentration fluctuation of the polymer phases: its orientation offers the largest chance for the two surface moieties to contacting with their favorable block segments. This implies that the structural formation kinetics is a cooperative event between these both “Janus” building blocks.

Upon the formation of the lamellar structures of polymers, the off-center interfacial distribution has come into being for the Janus nanoparticles (see the snapshots at 17000τ). Further calculation with a large time scale confirms that the deviation keeps almost unchangeable after the formation of the off-center interfacial nanostructure although the orientation of Janus nanoparticles still undergoes considerable fluctuation (Figure S8). Fundamentally, Janus nanoparticles can gain accessible more entropy through the orientational fluctuation.^{38,56} However, other entropic effects, such as the translational entropy of the deviated nanoparticles as well as the entropy gain from the disrupted orientation order of the stiff segments, contribute mainly to the off-center distribution of symmetric Janus nanoparticles.

Optical Properties. The heterogeneous materials formed by self-assembly of nanoparticles in block copolymers have the potential to produce promising photonic crystals due to the spatially periodic nanostructures.^{22,47} In photonic crystals, forbidden frequency bands, i.e., photonic band gaps, can be caused when incident electromagnetic waves are reflected and scattered by such regularly spaced regions of varying dielectric properties. Generally, the range of forbidden frequencies and the size of photonic band gaps are selective restricted, in line with the properties of the components within the system as well as the periodic structures.⁴⁷ As the spatial structure of Janus nanoparticle–block copolymer composites changes with the deviation of Janus nanoparticles from interfaces, one may anticipate that the optical properties of these systems can be extremely modified in response to various chain stiffness of the semiflexible block segment. By employing FDTD simulations, we thereby carry out the studies of the optical properties of these polymer nanocomposites in order to determine how changes of the interfacial nanostructures affect the optical properties of this heterogeneous media.

As schemed by the diagram of Figure 8a, a differentiated Gaussian pulse, encompassing a range of frequencies, is propagated toward the periodic structure of the nanocomposite.

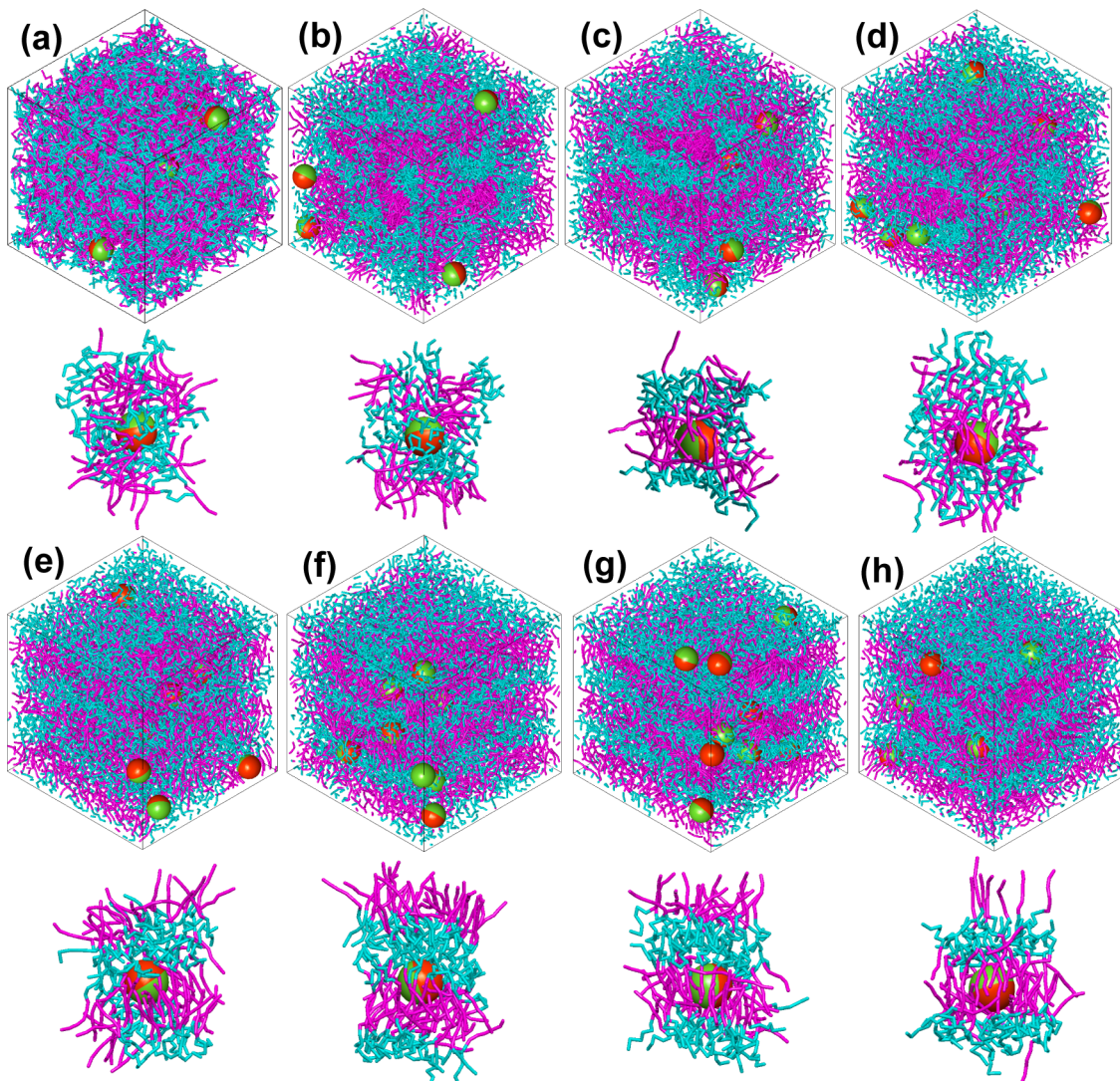


Figure 7. Representative simulation snapshots showing the kinetics pathway for the self-assembly of Janus nanoparticles in the AB diblock copolymers with flexible A block but stiff B block of $K_a = 100 k_B T$. The detailed structural organization of the polymer chains around a Janus nanoparticle is demonstrated at the bottom of each snapshot. The times of the simulation snapshots are (a) 0τ , (b) 200τ , (c) 1000τ , (d) 2000τ , (e) 4000τ , (f) 8000τ , (g) 14000τ , and (h) 17000τ .

Because of the one-dimensional nature of the structure, light of normal incidence (in the x -direction) will always propagate in the x -direction when reflected or transmitted from the structure. In the present simulations, all light is either reflected by the nanostructure or transmitted through it, being non-absorbing for the polymer nanocomposite. The frequencies that are forbidden to propagate through the structure can be examined by the fast Fourier transform (FFT) of the resultant transmitted and reflected signals. The transmitted and reflected spectra can be presented relative to the FFT of the original differentiated Gaussian pulse to give the normalized transmittance and reflectance. The transmittance spectra of a symmetric A_6B_6 diblock copolymer without the addition of fillers are shown in Figure S9, where a value of 1 in the vertical axis corresponds to 100% transmission. One can find that its principal frequency of reflectance occurs at about 0.89×10^{15} Hz, in agreement with the result estimated from theory.⁵⁷ Because of the small dielectric contrast in this system, the reflectance is small and the frequency band over which this reflectance occurs is also small.

We next turn to the nanocomposites of block copolymers that contain Janus nanoparticles. Considering the very small fraction of Janus nanoparticles used in the simulations, in the calculations of optical properties, we slightly increase the volume fraction of nanoparticles to a general concentration of about 10% while the volume fractions of blocks A and B are proportionally reduced according to the density profiles demonstrated in Figure 1e₁–e₅. Figure 8b presents the transmittance of these systems where the stiffness of B block segments is increased from $5 k_B T$ to $400 k_B T$ from bottom to top. The transmittance spectra are distinguished from the previous unfilled case in a number of ways. First, adding nanoparticles to the block copolymers enhances the dielectric contrast and thereby enlarges the magnitude of the reflectance and the size of the band gap. Indeed, the transmittance of light at certain frequencies is reduced to almost 0%; the width of the band gaps becomes larger, especially those corresponding to the higher orders of reflection. Second, the principal frequency of reflectance now enters into the optical range with $(3.8\text{--}7.9) \times 10^{14}$ Hz (as marked by the dotted vertical lines), corresponding to light in the visible spectrum.

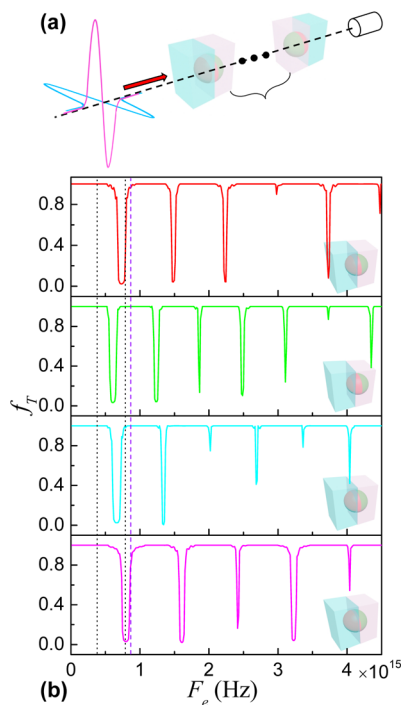


Figure 8. (a) Schematic diagram showing the structure of the FDTD simulation of the light propagating through the diblock copolymer-Janus particle nanocomposite. (b) Transmittance spectra from the FDTD simulation of AB diblock copolymers with flexible A block but stiff B block of various stiffness: (pink) $K_a = 5k_B T$, (cyan) $K_a = 60 k_B T$, (green) $K_a = 100 k_B T$, and (red) $K_a = 400 k_B T$. The dotted vertical lines mark the frequency range of visible spectrum. The violet dashed line denotes the principal frequency of the transmittance spectra of pure symmetric diblock copolymers. The insetting diagrams indicate the positions of Janus nanoparticle with respect to the phase interface at different K_a .

More interestingly, the principal frequency of reflectance demonstrates a definite dependence on the stiffness of B block segments: it migrates toward the red range of the visible spectrum when K_a is increased from $5 k_B T$ to $100 k_B T$ while crosses over to return to the violet range of the visible spectrum in the case of a further increase of K_a . Clearly, the optical response delicately reflects the stiffness-dependent behavior of the interfacial nanostructures as shown by Figures 1–3 and as illustrated by the insetting schematic diagrams of Figure 8b. Basically, a stiffer B block segments causes Janus nanoparticle to migrate toward the center of B domain, giving rise to a larger dielectric constant at these domains and thereby modifying the spectra. These results could have even greater implications; that is, by controlling the chain stiffness of one block segment, one could precisely tailor the band gaps and principal frequency of photonic crystals created by the self-assembly of nanoparticles in block copolymers.

CONCLUSION

In summary, we demonstrate novel chain stiffness-induced entropy effects that can be harnessed to tailor the precisely interfacial organization of Janus nanoparticles in the scaffold of block copolymers. The combination of techniques described above allows us to interrelate the spatial transition of interfacial nanostructures and the optical properties of the heterogeneous materials. It is found that the stiffness of the semiflexible block can regulate the off-center distribution of symmetric Janus nanoparticles with respect to the phase interface, featured by a

roughly 35% deviation from the interface to the utmost extent. The results reveal how entropic and enthalpic effects in this multiphase material contribute to the self-assembled morphologies and, in particular, can lead to entropically driven spatial transition of interfacial nanostructures. Our simulations demonstrate that the optical response, including the band gaps and principal frequency, delicately reflects the stiffness-dependent behavior of the interfacial nanostructures, suggesting an elegant approach to tailor the optical properties of the nanocomposite. This might be the very first simulation study to capture the chain stiffness-dependent spatial transition in the interfacial assembly of nanoparticles and thereby enables the applications of chain stiffness in precise control over the interfacial assembly of nanoparticles in polymer scaffolds. Furthermore, the nanostructure–optical property relation revealed here provides guidelines for facilitating the design of photonic band gap materials. Recalling the exquisite nanoscale-domain geometries of block copolymers with various molecular architectures⁵⁸ as well as the tailorabile surfaces and shapes of nanoparticles² (such as patchy particles), it would be interesting to explore to what extent the chain stiffness-induced entropy effects play a role in the control over the hierarchical structures and functionalities of the heterogeneous materials produced though the bottom-up assembly of such nano building blocks.

ASSOCIATED CONTENT

Supporting Information

Detailed discretization forms of FDTD and additional simulation results. The Supporting Information is available free of charge on the ACS Publications website at DOI: 10.1021/acs.macromol.5b01290.

AUTHOR INFORMATION

Corresponding Author

*E-mail: ltyan@mail.tsinghua.edu.cn (L.-T.Y.).

Notes

The authors declare no competing financial interest.

ACKNOWLEDGMENTS

The authors thank Junshi Liang, Pengyu Chen, Ce Lu, Guoxi Xu, and Chengcheng Ji for helpful discussions. This work is supported by the National Natural Science Foundation of China under Grants 21422403, 21174080, and 51273105.

REFERENCES

- (1) Balazs, A. C.; Emrick, T.; Russell, T. P. *Science* **2006**, *314*, 1107–1110.
- (2) Glotzer, S. C.; Solomon, A. J. *Nat. Mater.* **2007**, *6*, 557–562.
- (3) Frenkel, D. *Science* **2002**, *296*, 65–66.
- (4) Cademartiri, L.; Bishop, K. J. M. *Nat. Mater.* **2015**, *14*, 2–9.
- (5) Grzelczak, M.; Vermant, J.; Furst, E. M.; Liz-Marzan, L. M. *ACS Nano* **2010**, *4*, 3591–3605.
- (6) Tang, Z. Y.; Zhang, Z. L.; Wang, Y.; Glotzer, S. C.; Kotov, N. A. *Science* **2006**, *314*, 274–278.
- (7) Chen, Q.; Bae, S. C.; Granick, S. *Nature* **2011**, *469*, 381–384.
- (8) Liu, K.; Nie, Z.; Zhao, N.; Li, W.; Rubinstein, M.; Kumacheva, E. *Science* **2010**, *329*, 197–200.
- (9) Morgan, J. W. R.; Chakrabarti, D.; Dorsaz, N.; Wales, D. J. *ACS Nano* **2013**, *7*, 1246–1256.
- (10) Park, S. Y.; Lytton-Jean, A. K. R.; Lee, B.; Weigand, S.; Schatz, G. C.; Mirkin, C. A. *Nature* **2008**, *451*, 553–556.
- (11) Cigler, P.; Lytton-Jean, A. K. R.; Anderson, D. G.; Finn, M. G.; Park, S. Y. *Nat. Mater.* **2010**, *9*, 918–922.

- (12) Maye, M. M.; Kumara, M. T.; Nykypanchuk, D.; Sherman, W. B.; Gang, O. *Nat. Nanotechnol.* **2010**, *5*, 116–120.
- (13) Wang, Y.; Wang, Y.; Breed, D. R.; Manoharan, V. N.; Feng, L.; Hollingsworth, A. D.; Weck, M.; Pine, D. J. *Nature* **2012**, *491*, 51–55.
- (14) Kao, J.; Thorkelsson, K.; Bai, P.; Rancatore, B. J.; Xu, T. *Chem. Soc. Rev.* **2013**, *42*, 2654–2678.
- (15) Yan, L. T.; Xie, X. M. *Prog. Polym. Sci.* **2013**, *38*, 369–406.
- (16) Thompson, R. B.; Ginzburg, V. V.; Matsen, M. W.; Balazs, A. C. *Science* **2001**, *292*, 2469–2472.
- (17) Lin, Y.; Böker, A.; He, J.; Sill, K.; Xiang, H.; Abetz, C.; Li, X.; Emrick, T.; Long, S.; Wang, Q.; Balazs, A. C.; Russell, T. P. *Nature* **2005**, *434*, 55–59.
- (18) Liu, Z.; Guo, R.; Xu, G.; Huang, Z.; Yan, L. T. *Nano Lett.* **2014**, *14*, 6910–6916.
- (19) Hore, M. J. A.; Composto, R. J. *ACS Nano* **2010**, *4*, 6941–6949.
- (20) Aldaye, F. A.; Palmer, A. L.; Sleiman, H. F. *Science* **2008**, *321*, 1795–1799.
- (21) Chiu, J. J.; Kim, B. J.; Kramer, E. J.; Pine, D. J. *J. Am. Chem. Soc.* **2005**, *127*, 5036–5037.
- (22) Bockstaller, M. R.; Mickiewicz, R. A.; Thomas, E. L. *Adv. Mater.* **2005**, *17*, 1331–1349.
- (23) Deshmukh, R. D.; Liu, Y.; Composto, R. J. *Nano Lett.* **2007**, *7*, 3662–3668.
- (24) Zhao, Y.; Thorkelsson, K.; Mastroianni, A. J.; Schilling, T.; Luther, J. M.; Rancatore, B. J.; Matsunaga, K.; Jinnai, H.; Wu, Y.; Poulsen, D.; Frechet, J. M. J.; Alivisatos, A. P.; Xu, T. *Nat. Mater.* **2009**, *8*, 979–985.
- (25) Kao, J.; Bai, P.; Lucas, J. M.; Alivisato, A. P.; Xu, T. *J. Am. Chem. Soc.* **2013**, *135*, 1680–1683.
- (26) Kang, H.; Detcheverry, F. A.; Mangham, A. N.; Stoykovich, M. P.; Daoulas, K. C.; Hamers, R. J.; Müller, M.; de Pablo, J. J.; Nealey, P. F. *Phys. Rev. Lett.* **2008**, *100*, 148303.
- (27) Kim, J. U.; Matsen, M. W. *Phys. Rev. Lett.* **2009**, *102*, 078303.
- (28) Yan, L. T.; Popp, N.; Ghosh, S. K.; Böker, A. *ACS Nano* **2010**, *4*, 913–920.
- (29) Tay, K. A.; Bresme, F. *J. Am. Chem. Soc.* **2006**, *128*, 14166–14175.
- (30) Tao, A.; Sinsermsuksakul, P.; Yang, P. *Nat. Nanotechnol.* **2007**, *2*, 435–440.
- (31) Crossley, S.; Faria, J.; Shen, M.; Resasco, D. E. *Science* **2010**, *327*, 68–72.
- (32) Böker, A.; He, J.; Emrick, T.; Russell, T. P. *Soft Matter* **2007**, *3*, 1231–1248.
- (33) Garbin, V.; Jenkins, I.; Sinn, T.; Crocker, J. C.; Stebe, K. J. *Phys. Rev. Lett.* **2015**, *114*, 108301.
- (34) Walther, A.; Müller, A. H. E. *Chem. Rev.* **2013**, *113*, 5194–5261.
- (35) Frenkel, D. *Nat. Mater.* **2015**, *14*, 9–12.
- (36) van Anders, G.; Klotsa, D.; Ahmed, N. K.; Engel, M.; Glotzer, S. C. *Proc. Natl. Acad. Sci. U. S. A.* **2014**, *111*, E4812–E4821.
- (37) Sheiko, S. S.; Zhou, J.; Arnold, J.; Neugebauer, D.; Matyjaszewski, K.; Tsitsilianis, C.; Tsukruk, V.; Carrillo, J. M. Y.; Dobrynin, A. V.; Rubinstein, M. *Nat. Mater.* **2013**, *12*, 735–740.
- (38) Mao, X.; Chen, Q.; Granick, S. *Nat. Mater.* **2013**, *12*, 217–222.
- (39) De Nijs, B.; Dussi, S.; Smalenburg, F.; Meeldijk, J. D.; Groenendijk, D. J.; Filion, L.; Imhof, A.; van Bladderen, A.; Dijkstra, M. *Nat. Mater.* **2015**, *14*, 56–60.
- (40) Zhang, D.; Carignano, M. A.; Sleifer, I. *Phys. Rev. Lett.* **2006**, *96*, 028701.
- (41) Groot, R. D.; Warren, P. B. *J. Chem. Phys.* **1997**, *107*, 4423–4435.
- (42) Allen, M. P.; Tildesley, D. J. *Computer Simulation of Liquids*; Clarendon Press: Oxford, 1987.
- (43) Micka, U.; Kremer, K. *J. Phys.: Condens. Matter* **1996**, *8*, 9463–9470.
- (44) Yee, S. K. *IEEE Trans. Antennas Prop.* **1966**, *AP-14*, 302–307.
- (45) Maxwell, J. C. *Philos. Trans. R. Soc. London* **1865**, *155*, 459–512.
- (46) Berenger, J. P. *J. Comput. Phys.* **1996**, *127*, 363–379.
- (47) Edrington, A. C.; Urbas, A. M.; DeRege, P.; Chen, C. X.; Swager, T. W.; Hadjichristidis, N.; Xenidou, M.; Fetter, L. J.; Joannopoulos, J. D.; Fink, Y.; Thomas, E. L. *Adv. Mater.* **2001**, *13*, 421–425.
- (48) *CRC Handbook of Chemistry and Physics*, 83rd ed.; CRC Publishing Co.: New York, 2003.
- (49) Baranyai, A.; Evans, D. J. *Phys. Rev. A: At., Mol., Opt. Phys.* **1989**, *40*, 3817–3822.
- (50) Goel, T.; Patra, C. N.; Mukherjee, T.; Chakravarty, C. *J. Chem. Phys.* **2008**, *129*, 164904.
- (51) Chen, J. T.; Thomas, E. L.; Ober, C. K.; Mao, G. P. *Science* **1996**, *273*, 343–346.
- (52) Kumar, N. A.; Ganesan, V. *J. Chem. Phys.* **2012**, *136*, 101101.
- (53) Jiang, Y.; Chen, J. Z. *Y. Phys. Rev. Lett.* **2013**, *110*, 138305.
- (54) Hsin, J.; Gumbart, J.; Trabuco, L. G.; Villa, E.; Qian, P.; Hunter, C. N.; Schulter, K. *Biophys. J.* **2009**, *97*, 321–329.
- (55) Dong, B.; Guo, R.; Yan, L. T. *Macromolecules* **2014**, *47*, 4369–4379.
- (56) Jiang, S.; Yan, J.; Whitmer, J. K.; Anthony, S. M.; Luijten, E.; Granick, S. *Phys. Rev. Lett.* **2014**, *112*, 218301.
- (57) Buxton, G. A.; Lee, J. Y.; Balazs, A. C. *Macromolecules* **2003**, *36*, 9631–9637.
- (58) Bates, F. S.; Hillmyer, M. A.; Lodge, T. P.; Bates, C. M.; Delaney, K. T.; Fredrickson, G. H. *Science* **2012**, *336*, 434–440.